Hindawi
Mathematical Problems in Engineering
Volume 2024, Article ID 8313135, 17 pages
https://doi.org/10.1155/2024/8313135

Research Article

An Analytical-Based Lightning-Induced Damage Model for an Aircraft Wing Exposed to Pressure Loading of Lightning

Aysun Soysal,[1] **Ibrahim Ozkol**,[2] **and Erol Uzal**[3]

[1]*Department of Mathematical Engineering, İstanbul Technical University, İstanbul, Türkiye*
[2]*Department of Aerospace Engineering, İstanbul Technical University, İstanbul, Türkiye*
[3]*Department of Mechanical Engineering, İstanbul University-Cerrahpasa, İstanbul, Türkiye*

Correspondence should be addressed to Aysun Soysal; soysal17@itu.edu.tr

Received 16 October 2023; Revised 22 December 2023; Accepted 2 January 2024; Published 27 January 2024

Academic Editor: Francisco Rossomando

Lightning is one of the natural hazards that any aircraft may encounter while navigating. If adequate precautions are not taken against lightning, structural damage, operational disruptions, and loss of life and property can occur. Thus, studying the mechanism of damage caused by lightning strikes in an aircraft's structural material is necessary to optimize the structure, minimize the damage, and reduce the cost caused by lightning. In the present article, the lightning-induced damage behavior of an aircraft structural material was investigated from an analytical perspective. For this purpose, two analytical-based models were developed: an improved electromagnetic pressure impact model (IEPIM) and the damage model in an aircraft wing. For the IEPIM, the findings of the article showed that the proposed pressure model is in good agreement with the experimental studies, borrowed from the open literature, for 100 and 200 kA lightning current. For the damage model, the findings of the article indicated that (i) even though lightning strikes to the regions with the same characteristics on an aircraft wing in terms of the lightning strike zone, the amount of deflection in the wing increases as the impact point approaches the wing tip and decreases as it approaches the wing root, (ii) without changing the lightning strike point (x_0), when the damping coefficient (ξ) is increased in the range of $[0, 2\xi]$, the amount of deflection decreases as the amount of damping coefficient increases, and (iii) when lightning with a current of 100 kA hits to the wing root of an aircraft, the pressure impact of the lightning causes more torsion deflection than bending deflection at the wing root; however, when it hits to the mid-wing or wing tip of an aircraft, the pressure impact of the lightning causes more bending deflection than torsion deflection at the mid-wing or wing tip.

1. Introduction

In recent years, air transportation has played a very important role in both global economic growth and traveling long distances in a shorter time. However, one of the common occurrences that any aircraft encounters during air transportation is lightning strikes. Moreover, the threat can be even more critical for aircrafts that must fly at low altitudes and weather-independent conditions, where the lightning risk is greatest. Past lightning events and aircraft accidents revealed that the impact of lightning can result in structural damage [1], operational disruptions [2], and loss of life and property [3]. Furthermore, in recent years, it has been stated that the flying ring cost of lightning-caused disruptions (e.g., delays and cancelations) can be nearly five times the cost of replacing an existing facility [4]. Therefore, the influence of the impact of lightning on aircraft structural materials must be investigated not only to determine and minimize the lightning-induced damages but also to reduce the cost caused by lightning, which contributes to the procedures for the design, production, and certification standards [5] of civil and commercial aircrafts.

A lightning event arises once a supercooled liquid and ice particles above freezing encounter. As a result of this event, large-and-distinct positive and negative electric charges in the clouds arise. Then, the lightning current discharge starts, and an intense current of around 30,000 amps' flows through the arc channel of lightning [6]. If an aircraft is exposed to an intense current, a large amount of energy is transmitted to one of the front extremities of the aircraft (such as the

Table 1: Pressure loading of lightning in the existing literature.

Author	Formulation of pressure loading of lightning
Kawakami [10]	$P(r,t) = \mu_0 I^2(t)/8\pi^2 r_c^2$
Chemartin et al. [15]	$P(r,t) = \mu_0 I^2(t)/4\pi^2 r^2$
Muñoz et al. [13]	$P(r,t) = \begin{cases} \mu_0 I^2(t)/4\pi^2 r_c^2, & r < r_c \\ \mu_0 I^2(t)/4\pi^2 r^2, & r > r_c \end{cases}$
Martins [11]	$P(0,t) = P_1 e^{-t/\tau_1} + P_2 e^{-t/\tau_2}$
Karch et al. [12]	$P(r,t) = (\mu_r \mu_0 I^2(t)/4\pi)[\frac{1}{4} + \ln(r_c/R_r(t))]$
Lee et al. [14].	$P(r,t) = -\mu_0 I^2(t)/8\pi^2 r_c^2$

radome [7], fuselage [8], wing tip [9], etc.) and then exits from another extremity (e.g., tail) of the aircraft. The air around the structural part of the aircraft exposed to lightning begins to ionize, and then the electromagnetic field intensity increases in this part, which generates a pressure impact. Thereafter, the wave of the pressure coming from the arc channel of the lightning propagates by acting as axial, lateral, and radial pressure on nearby structures [10].

Some authors [10–15] in the literature studied with the lateral pressure loading of lightning as a transverse force applied to a structure in the thickness direction of the structure by using different approaches. While some of them pointed out that lateral pressure loading is electromagnetic (or magnetic) pressure [10–12], others suggested that lateral pressure loading is a resultant pressure that consists of electromagnetic and acoustic pressure [13–15]. The modeling approaches proposed by the authors are given in Table 1. The findings of the studies of the authors indicated that when the arc channel of lightning attaches to the surface of a structure, the radius of the arc channel expands over time, which supports that the radius of the arc channel is time-varying. Moreover, once any structural part of an aircraft is subjected to a lightning strike, while the arc channel of lightning stands in its initial position, the aircraft travels forward a significant distance during the flash lifetime [16]. Therefore, although lightning hits to a single point on the aircraft structure, the lightning currents [17] and pressure effect [10] of lightning are distributed over the aircraft structure. As seen in Table 1, in the modeling approaches of the lateral pressure loading of lightning, some of the authors considered the distributed pressure effect of lightning but neglected the time-varying radius of the arc channel in the model. On the other hand, some took into account the time-varying radius of the arc channel but ignored the distributed pressure effect of lightning. Although these modeling approaches gave relatively acceptable and reasonable results, new modeling approaches are always possible to represent the natural behavior of lightning. For instance, introducing a model, that includes both the distributed pressure effect and time-varying radius of the arc channel of lightning, would be a good advance in modeling the pressure impact of lightning. Lightning is a multi-physical phenomenon [18, 19], although it is almost impossible to fully understand its nature, improvements are always possible.

In Table 1, μ_0 is the magnetic permeability, $\mu_0 = 4\pi \times 10^{-7}\ N/A$; $I(t)$ is the lightning current; r_c is the time-invariant radius of the arc channel of lightning; r is the radial distance to the lightning strike attachment point; P_1 and P_2 are coefficients and τ_1 and τ_2 are time constants; μ_r is the relatively permeability of the nonmagnetic lightning protection, $\mu_r = 1$; $R_r(t)$ is the value of the radius of arc root, and t is time.

Since lightning strike is a threat to all aircraft structures made of metallic or composite material, numerous experimental and numerical studies were covered in the literature to investigate the damage behavior of aircraft structural materials exposed to pressure loading of lightning. Among the experimental studies, Damghani et al. [20] examined the effects of transverse impact loading of lightning on two laminate configurations to determine the shear-buckling behavior of the laminate. Boushab et al. [21] studied the lightning damage resistance of a carbon-epoxy panel by considering lightning arc channel expansion to find out the cause of the widespread surface damage. Guerrero et al. [22] analyzed a carbon-aluminum wing box subjected to the loading of lightning to improve the structural behavior of the wing box. Although experimentation is the safest way to solve an engineering problem, providing reasonably good experimental solutions to the lightning problems for aircraft structural materials in the appropriate physical environment and under ideal conditions can be quite burdensome, both financially and temporally. To overcome such difficulties, some numerical models of lightning-induced damages in aircraft structural materials were proposed in the literature. Lee et al. [23] predicted the mechanical damage caused by the impact of lightning by considering the shock wave overpressure and lightning arc channel expansion via the finite element method. Foster et al. [24] investigated the potential contribution of lightning pressure loading to composite sample damage in terms of the form and scale of damage. Bigand et al. [25] proposed a numerical model of the damage caused by the overpressure of a lightning strikes on an aircraft composite structure protected with a metallic mesh and painted. Qian et al. [26] realized the simulation of a turbofan engine of an aircraft encountering a lightning strike to investigate the electromagnetic effect of lightning strike on motor control cables by using CST software based on the transmission line matrix method in the simulation. In spite of progress that was made in the experimental studies to model lightning-induced damages in aircraft structural materials, a complete analysis is almost impossible under current technological conditions because of the multiphysical nature of lightning [27]. Furthermore, despite the tremendous development of computers and numerical algorithms, it is also impossible to solve the lightning problem numerically today [28]. However, by simplifying engineering structures under some assumptions, utilizing the power of analytical modeling can be a guide in solving engineering problems. Moreover, even if it may seem unfeasible to understand the relationships between different parameters of a structure and forces that influence a particular outcome, analytical modeling is an effective and reliable technique for turning many different variables and conditions into information one can use.

The present article is an extended version of the article published in [29]. The goal of the present article is to investigate the lightning-induced damage behavior of an aircraft

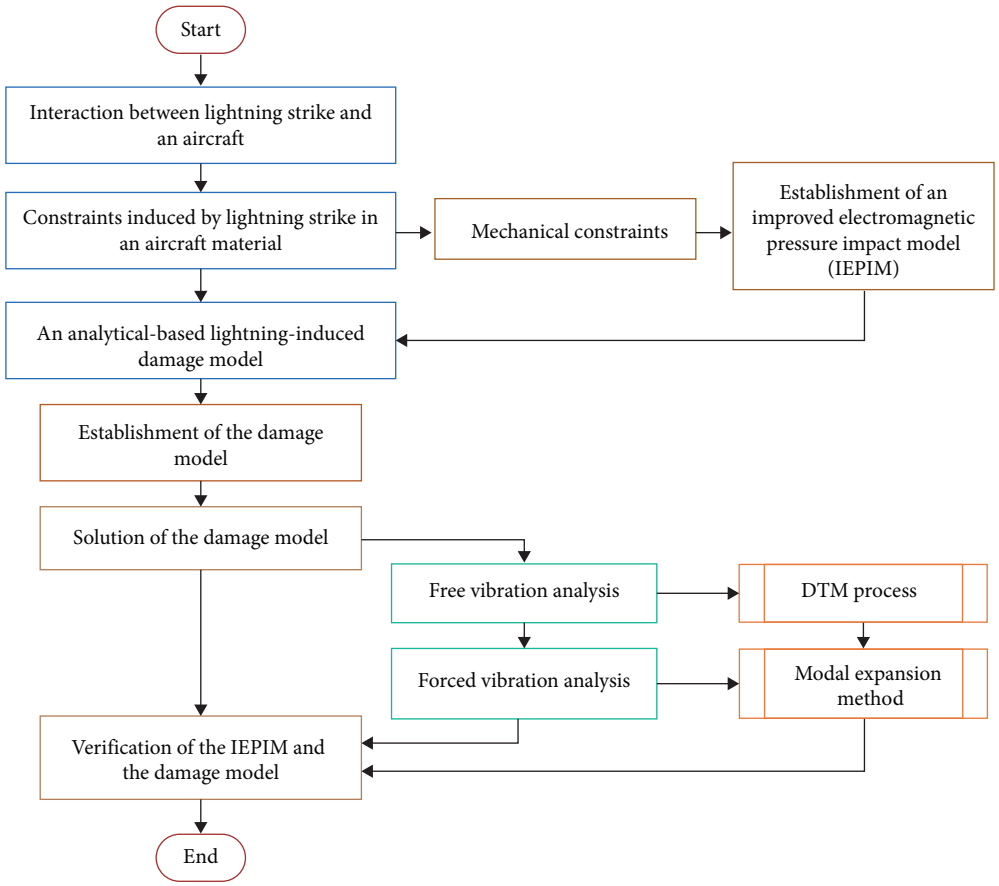

Figure 1: A diagram that summarizes the stages of the present study.

structural material from an analytical perspective. For this purpose, two analytical-based models are proposed. The first is for the pressure loading of lightning, which is named the improved electromagnetic pressure impact model (IEPIM); the latter is for the damage in an aircraft wing exposed to the pressure loading of lightning, which is named the damage model in the rest of the present article. In this context, first, the IEPIM is established. Second, with the help of the IEPIM, the damage model is established. In the solution of the damage model, free vibration analysis by using the differential transform method (DTM) and forced vibration analysis by using the modal expansion method are conducted. The results of the theoretical formulations developed in the present article are obtained with codes developed by the user in the MATLAB environment. Then, to verify the models established, the results of the models are compared with the results of some experimental studies borrowed from the open literature where comparison is possible. A diagram summarizing the stages of the present article is given in Figure 1.

2. Materials and Methods

2.1. Interaction between Lightning Strike and an Aircraft. Due to unexpected hazards and serious accidents caused by lightning strikes on aircrafts, aviation regulatory bodies around the world have established certification standards to ensure that aircrafts can withstand lightning strikes and land safely at a suitable airport at the end of the flight. Considering the certification standards established, modern aircraft manufacturers have used various lightning protection systems to prevent and/or reduce potential direct and indirect hazards caused by lightning strikes. The main purpose of protecting an aircraft's fuselage and structures is to identify areas on the aircraft that are most vulnerable to lightning strikes. Thus, the surface of the aircraft can be classified as a function of the lightning threat, which results in the information about the intensity of lightning and the extent of damage in the aircraft.

Based on vulnerability to lightning, the division of surface of aircrafts into lightning strike zones may vary depending on some factors such as the aircrafts' intended use, geometry, and how often they are flown, etc.; however, the major standards are similar for most aircrafts. In the open literature, the lightning strike zones for aircrafts were determined according to the Aerospace Recommended Practice (ARP) 5414 standards of the Society of Aerospace Engineers (SAE) [13]. The lightning strike zones for an aircraft wing are shown in Figure2 [30], and the descriptions of these zones are given in Table 2 [31].

Based on experimental studies, a lightning current was formulated as the following expression [11, 12]

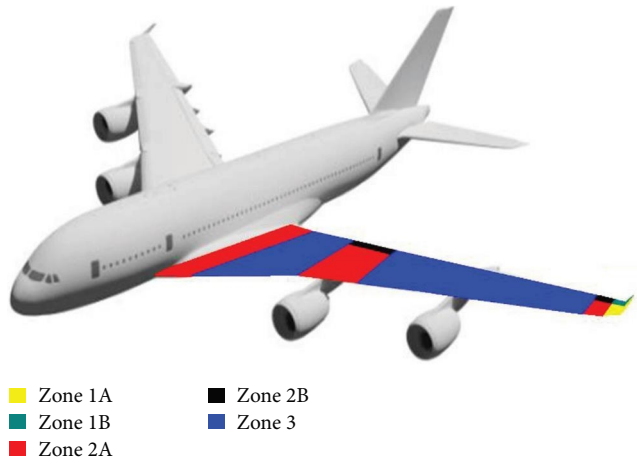

Figure 2: Dividing an aircraft wing into zones based on its sensitivity to lightning strikes.

Table 2: Descriptions of lightning strike zones on an aircraft wing.

Zones	Descriptions of lightning strike zones
Zone 1A	Initial attachment point with low possibility of lightning channel hang-on
Zone 1B	Initial attachment point with high possibility of lightning channel hang-on
Zone 2A	Swept stroke zone with low possibility of lightning channel hang-on
Zone 2B	Swept stroke zone with high possibility of lightning channel hang-on
Zone 3	Areas not in Zone 1A, 1B, 2A, or 2B, where damage least probable

$$I(t) = I_0(\exp(-\alpha t) - \exp(-\beta t)), \quad (1)$$

where α and β are parameters, and their values change depending on the lightning current components that are A, B, C, and D, as shown in Table 3 [32]. The durations and amplitudes of the components are shown in Figure 3 [10]. In addition, the relationships between lightning current components and lightning strike zones are given in Table 4 [1, 10].

2.2. Constraints Induced by Lightning Strike on an Aircraft Material. Aircrafts can trigger lightning while flying through a charged cloud. Once the trigger starts, the lightning process begins. One of the main stages of this process is the leading stage [30]. The leading stage is the onset and development of a conductive arc channel of lightning. After the arc channel is developed, lightning discharges begin to flow through the arc channel. The lightning discharges are grouped depending on the beginning and ending of the discharges, which are intracloud, cloud-to-ground, and cloud-to-cloud discharges [33]. The most common type of lightning discharge is cloud-to-ground, which accounts for 90% of all lightning strikes [34]. The percentage of the form of lightning discharge varies depending on the storm in the current geography [35]. However, according to the findings of a study [35], it was revealed that single-lightning flashes are much more common among lightning flashes recorded by lightning detection systems. Even if a single lightning flash hits to an aircraft in flight, the lightning flash has an impact, including thermal [12], electrical [14], and mechanical [11] effects. These effects of lightning can be broadly divided into two categories: thermo-mechanical constraints and electromagnetic constraints. The thermal–mechanical constraints relate to the damage to the airframe materials and can lead to destructive effects such as vibrations that resonate the structure [36], rupture of the extremities of the aircraft [1], pitting [37], deflection [38], etc. Conversely, the electromagnetic constraints relate to the damage to any electronic system, causing interference to the electronic equipment on board and thus leading to computer control systems malfunction [39].

2.2.1. Mechanical Constraints Caused by Electromagnetic Pressure Impact. Figure 4 shows the life cycle of damage caused by a single-lightning strike on an aircraft wing made of a metallic material. As shown in Figure 4, if the material of an aircraft wing exposed to a lightning strike has high thermal and electrical conductivity, the electrical and thermal energy generated by the lightning strike are swept from the wing and given back to the air [30]; and therefore, if negligible local thermal effects coming from the energy conversion are not considered, only mechanical constraints caused by the pressure impact of lightning occur in the area struck by lightning. At this stage, the arc channel of lightning interacts with the surface of the aircraft wing, and then the radius of the arc channel expands over time

Table 3: Values of the lightning current parameters.

Lightning current components	I_0 (Amper)	α (s^{-1})	β (s^{-1})
A	218,810	11,354	647,265
B	11,300	700	2,000
C	400	Not applicable	Not applicable
D	109,405	22,708	1,294,530

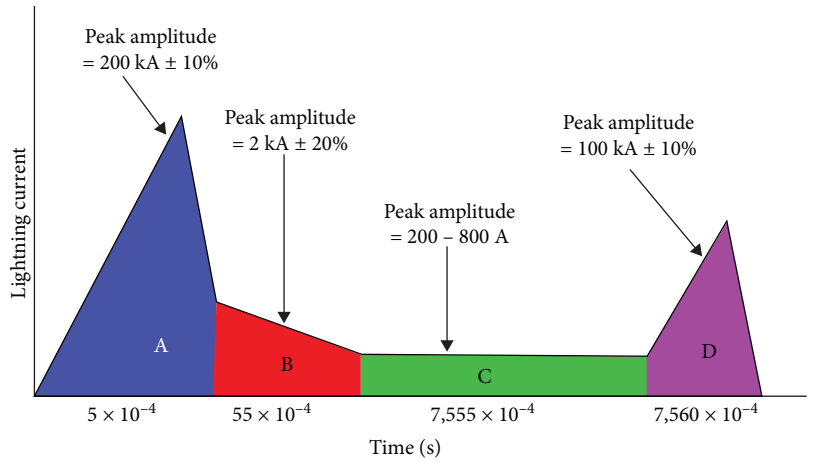

Figure 3: Duration and amplitude of the lightning current components.

Table 4: Relations between lightning strike zones and lightning current components.

Lightning strike zone	Lightning current components
Zone 1A	A + B
Zone 1B	A + B + C + D
Zone 2A	B + D
Zone 2B	B + C + D
Zone 3	A + D

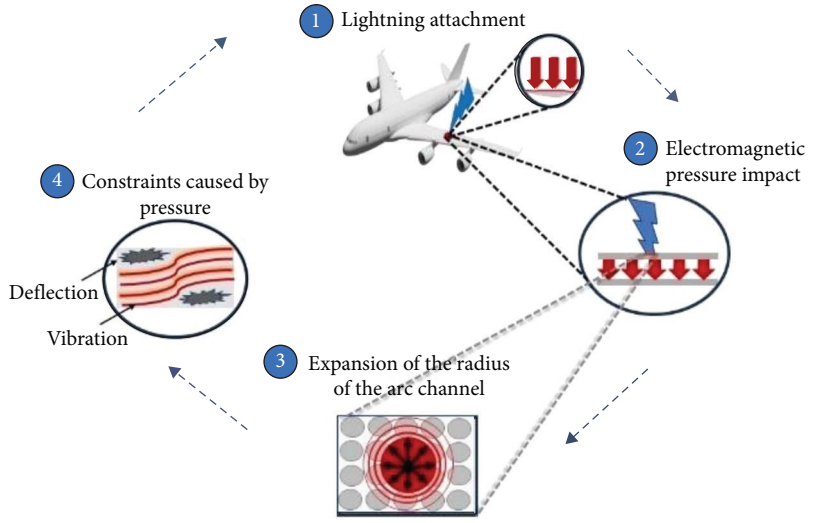

Figure 4: Life cycle of damage in an aircraft wing struck by lightning.

[5, 11–15]. During this time, the magnetic interaction occurs between the current flow in the arc channel and the current flow on the surface of the aircraft wing. Then, this interaction exerts an impulsive force on the surface of the aircraft wing [13], which generates the pressure waves propagating from the arc channel by acting on nearby structures [10]. The lateral pressure waves arising in the expanding arc channel contribute significantly to the mechanical constraints [13], including elastic displacements, deflection, etc.

One of the factors affecting lightning-induced damage in a structure is the slenderness of the structure. For thinner structures with a high slenderness ratio, such as cables, the effect of the pressure enhances by the slenderness ratio, so that even low-pressure states far from the buckling stage may have a significant impact on the dynamics of the structure [40]. For instance, when an overhead ground wire that has a high slenderness ratio (almost all 1D structure) and is generally made of an aluminum-clad steel strand [41] is struck by lightning, thermal ablation damage [42] or rupture accident [43] can occur in the structure. However, due to mission requirements, aircrafts present high-aspect-ratio wings that result in relatively flexible structures [44]. Therefore, the high flexibility and large aspect ratios can cause large deflections of up to approximately 25% of the wing half-span [45] rather than rupture hazards or thermal ablation.

During lightning strikes, another source of mechanical constraints is acoustic overpressure [13]. Lightning releases substantial amounts of energy into a quite narrow volume of air in a very short period [46]. Thereby, the air in the ionized lightning arc channel is heated to extremely high temperatures almost instantly [47], hence arising high pressures of the expanding plasma in the arc channel [10]. This pressure generates radial pressure and resulting shock waves in the heated channel [48]. Then, the shock waves expand and propagate radially outwards from the center of the discharge channel, leading to mechanical constraints in the structures, especially in the structures that are more sensitive to breakage (e.g., composite skin) [13]. In this article, the acoustic pressure propagating in radial directions of the ionization channel is neglected, and only the lateral pressure effect (i.e., EPI) is considered due to the subject of the article.

2.2.2. Establishment of an Improved Electromagnetic Pressure Impact Model (IEPIM). According to some studies [49], the radius of the arc channel of lightning can be modeled as a function of response time as follows:

$$r_c(t) = \alpha_0 \rho_0^{-1/6} [I(t)]^{1/3} t^{1/2}, \tag{2}$$

where $r_c(t)$ is radius of the arc channel (m) expanding in time, α_0 is constant, $\alpha_0 = 0.102$, ρ_0 is the air density at atmosphere pressure, and $\rho_0 = 1.29\ \mathrm{kg/m^3}$, $I(t)$ is lightning current.

Muñoz et al. [13] considered the distributed pressure effect of lightning with a time-invariant radius of the arc channel in the pressure model. To propose an IEPIM involving not only the distributed pressure effect of lightning but also the time-dependent radius of the arc channel, the time-dependent radius of the arc channel given in Equation (2) is combined with the pressure model of lightning, which is also given in Table 1, in [13]. The radial distance relative to the lightning strike point, r, can be reexpressed in terms of the strike point on the wing as $L - x$ in the formulation of the pressure. Therefore, an IEPIM of lightning is obtained as follows:

$$P_G(x,t) = \begin{cases} \dfrac{\mu_0 I^{\frac{4}{3}}(t)}{4\pi^2 \alpha_0^2 \rho_0^{-1/3} t}, & x \le L - 2r_c \\ \dfrac{\mu_0 I^2(t)}{4\pi^2 (L-x)^2}, & x < L - 2r_c \end{cases}, \tag{3}$$

where x denotes any point of a structure subjected to the pressure loading of lightning, L is the length of the structure, and r_c is the maximum point reached by the radius of the arc channel of lightning.

In the next section, by using the IEPIM expressed in Equation (3), an analytical model of the damage caused by the pressure loading of lightning in an aircraft wing is established to investigate the lightning-induced damage behavior of the aircraft wing material. In the damage model to be established, a single cloud-to-ground type lightning strike is considered because it is more common and more observable in nature [34, 35].

2.3. An Analytical-Based Lightning-Induced Damage Model

2.3.1. Establishment of the Model. One of the most vulnerable locations to lightning strikes is the wing of most aircrafts [50]. In the construction of an aircraft wing and examination of its resistance deviation against static and dynamic loads, beam structures can be used [15, 18]. Especially, beams, which are clamped at the origin of the body axes and have coupled bending and torsional behavior, are good approaches to aircraft wing structures [17]. For this reason, in the establishment of an analytical model of the lightning-induced damage in an aircraft wing, an average uniform aircraft wing structure made of a material with high thermal and electrical conductivity is considered a bending–torsion coupled beam while the pressure loading of lightning is modeled as a flexural loading applied to the beam.

It should be noted that when lightning hits to an aircraft wing material, the constraints caused by the lightning strike in the material occur in a time interval of the order of microseconds [51]; for this reason, the effects of the aerodynamic forces, which are the forces acting on the body moving through the air such as lift, drag, and downforce in the air, can be negligible in this process. Moreover, the local heat effects caused by the energy conversion are not included in the model since these effects are quite small when compared with the mechanical effects in an aircraft wing. Furthermore, due to the subject of the study, the other parts (such as rips, spars, engines, or avionics systems) of the wing structure are not included in the damage model.

The partial differential equations and boundary conditions of the damage model in an aircraft wing subjected to the pressure loading of lightning are given in Equations (4)–(8). Here, $u(x,t)$ is bending translation in the vertical direction and $\psi(x,t)$ is torsional rotation about the elastic axis of the wing, where x

denotes distance from the origin and t denotes time. Moreover, EI, GJ, m, x_α, and I_α are, respectively, bending rigidity, torsional rigidity, the mass of the wing per unit length, bending–torsion coupling term, and mass moment of inertia per unit length of the wing about the elastic axis; the coefficients c_1 and c_2 are the linear viscous damping terms of per unit length of the wing in bending deformation and torsional deformation, respectively; $(\,')$ and $\dot{(\,)}$ denote, respectively, differentiations with respect to space x and time t.

$$EIu'''' - c_1(\dot{u} - x_\alpha\dot{\psi}) - m(\ddot{u} - x_\alpha\ddot{\psi}) = P_G(x,t), \tag{4}$$

$$GJ\psi'' - c_2\dot{\psi} + c_1x_\alpha\dot{u} - I_\alpha\ddot{\psi} + mx_\alpha\ddot{u} = 0, \tag{5}$$

$$u = u' = \psi = 0 \text{ at } x = 0, \tag{6}$$

$$u'' = u''' = \psi' = 0 \text{ at } x = L, \tag{7}$$

with

$$P_G(x,t) = \begin{cases} \dfrac{\mu_0 I^{\frac{4}{3}}(t)}{4\pi^2\alpha_0^2\rho_0^{-1/3}t}, & x \le L - 2r_c \\ \dfrac{\mu_0 I^2(t)}{4\pi^2(L-x)^2}, & x < L - 2r_c \end{cases}, \tag{8}$$

2.3.2. Solution of the Model.

(1) Free vibration analysis. For undamped free vibration analysis, the external distributed force $P_G(x,t)$ and the damping coefficients c_1 and c_2 are set to zero to determine the dynamic characteristics (i.e., vibration frequency and vibration mode shapes) of the aircraft wing model stated in Equations (4)–(8). In harmonic oscillation, $u(x,t)$ and $\psi(x,t)$ are approximated by a sinusoidal variation with circular vibration frequency ω_n as follows:

$$u(x,t) = U_n(x)e^{i\omega_n t}, \tag{9}$$

$$\psi(x,t) = \Psi_n(x)e^{i\omega_n t}, \tag{10}$$

where $U_n(x)$ and $\Psi_n(x)$ are, respectively, amplitudes of the sinusoidal variation of the bending displacement and torsional rotation of the wing, and $n = 1, 2, 3, \ldots$.

Substituting Equations (9) and (10) into Equations (4)–(7) gives the ordinary differential equations and related boundary conditions as follows:

$$U_n'''' - aU_n + c\Psi_n = 0, \tag{11}$$

$$\Psi_n'' + b\Psi_n - dU_n = 0, \tag{12}$$

$$U_n = U_n' = \Psi = 0 \text{ at } x = 0, \tag{13}$$

$$U_n'' = U_n''' = \Psi_n' = 0 \text{ at } x = L, \tag{14}$$

where $(\,') = d/dx$ and the coefficients $a, b, c,$ and d are as follows:

$$a = (m\omega_n{}^2)/EI, b = (I_\alpha\omega_n{}^2)/GJ, \tag{15}$$

$$c = (mx_\alpha\omega_n{}^2)/EI, d = (mx_\alpha\omega_n{}^2)/GJ. \tag{16}$$

Then, DTM is applied to solve the ordinary differential equations with associated boundary conditions given in Equations (11)–(14). According to the theory of DTM [52], an analytical function $f(x)$ is expanded to a power series with the center η_0 in the domain of $f(x)$. Thus, the differential transform and inverse transform of $f(x)$ are stated by $F_D[k]$ and $f_D[x]$, respectively, as follows [52]:

$$F_D[k] = \frac{1}{k!}\left(\frac{d^k f(x)}{dx^k}\right)\Bigg|_{x=\eta_0}, \tag{17}$$

$$f_D[x] = \sum_{k=0}^{\infty}(x - \eta_0)^k F_D[k], \tag{18}$$

The transformation rules of DTM for different functions and operations are given in [53]. After applying the transformation rules to both the ordinary differential equations and the boundary conditions, a set of algebraic equations is obtained as follows:

$$U_D[k+4] = \frac{aU_D[k] - c\Psi_D[k]}{(k+1)(k+2)(k+3)(k+4)}, \tag{19}$$

$$\Psi_D[k+2] = \frac{dU_D[k] - b\Psi_D[k]}{(k+1)(k+2)}, \tag{20}$$

$$U_D[0] = U_D[1] = \Psi_D[0] = 0 \quad \text{at } x = 0, \tag{21}$$

$$\sum_{k=0}^{N} k(k-1)U_D[k]L^{k-2} = 0 \quad \text{at } x = L, \tag{22}$$

$$\sum_{k=0}^{N} k(k-1)(k-2)U_D[k]L^{k-3} = 0 \quad \text{at } x = L, \tag{23}$$

$$\sum_{k=0}^{N} k\Psi_D[k]L^{k-1} = 0 \quad \text{at } x = L, \tag{24}$$

where $U_D[k]$ and $\Psi_D[k]$ are, respectively, the differential transform of $U_n(x)$ and $\Psi_n(x)$. In addition, in Equations (22)–(24), N denotes the number of terms included in the application of DTM, and its value is determined depending on the convergence of the vibration frequencies.

Subsequently, using the inverse transform formulation given in Equation (18), the vibration mode shapes of the wing are obtained as follows:

$$U_n(x) = \sum_{k=0}^{N} U_D[k]x^k, \tag{25}$$

$$\Psi_n(x) = \sum_{k=0}^{N} \Psi_D[k]x^k. \tag{26}$$

The Equations (25) and (26) are the conjunction with the boundary conditions. Furthermore, the orthogonality condition

Step 1. Read the data $EI, GJ, m, x_\alpha, I_\alpha, L$.
Step 2. Compute coefficeints a, b, c, d.
Step 3. Set $\mathrm{U}_D[i] = \alpha, U_D[i+1] = \beta, \Psi_D[i] = \gamma,\ i = 0, 1, 2, 3.$
For $k = 0, \ldots, N$
Compute $\mathrm{U}_D[k+4]$
Compute $\Psi_D[k+2]$
End
For $k = 0, \ldots, N$
Compute BC1
Compute BC2
Compute BC3
End
Step 4. Solve the following system of equations:

$$M_{j1}^{(n)}(\omega)\alpha + M_{j2}^{(n)}(\omega)\beta + M_{j3}^{(n)}(\omega)\gamma = 0, \quad j = 1, 2, 3.$$

Step 5. Check the convergence of the solution of the system given in Step 4.

$$|\omega_j^{(n)} - \omega_j^{(n-1)}| \le \varepsilon$$

where $\omega_j^{(n)}$: the *jth* estimated vibration frequency corresponding to n,
$\omega_j^{(n-1)}$: the *jth* estimated vibration frequency corresponding to $n-1$.
If iterative refinement is needed, go back to Step 5.
Step 6. Select the real parts of the vibration frequencies obtained in Step 5 as the resulting vibration frequencies.
Step 7. Compute the vibration mode shapes $\mathrm{U}_n(x)$ and $\psi_n(x)$ by using inverse transformation functions.

Algorithm 1: The pseudocode for application of DTM (ε : is a tolerance value, BC: boundary condition).

can be stated for different vibration mode shapes as follows [54]:

$$\int_0^L [(mU_mU_n + I_\alpha \Psi_m \Psi_n) - mx_\alpha(U_n\Psi_m + U_m\Psi_n)]d\xi = \mu_n \delta_{mn}, \tag{27}$$

where μ_n is the generalized mass in the nth mode and δ_{mn} is the Kronecker delta function. The pseudocode related to the application steps of DTM is given in Algorithm 1.

(2) Forced vibration analysis. In the forced vibration analysis, the modal expansion method is implemented. In this method, the solutions of the Equations (4)–(8) are approximated as follows:

$$u(x,t) = \sum_{n=1}^{\infty} q_n(t)U_n(x), \tag{28}$$

$$\psi(x,t) = \sum_{n=1}^{\infty} q_n(t)\Psi_n(x), \tag{29}$$

and the external flexural loading is assumed in the following form:

$$P_G(x,t) = D(x)f(t), \tag{30}$$

where $U_n(x)$ and $\Psi_n(x)$ are the vibration mode functions, $q_n(t)$ is a time-dependent generalized coordinate for the nth mode; $D(x)$ denotes the spatial distribution, and $f(t)$ denotes the time-dependent function factor of the external flexural load.

Substitution of Equations (28) and (29) into Equations (4) and (5), multiplication the final equations by $U_m(x)$ and $\Psi_m(x)$, addition the last two equations and then integration the last equation from 0 to L, along with the use of the orthogonality property of the mode functions given in Equation (27) results in the following equation in the modal coordinates:

$$\ddot{q}_n(t) + 2\xi_n\omega_n\dot{q}_n(t) + \omega_n^2 q_n(t) = F_n(t), \tag{31}$$

where ξ_n is the nondimensional damping coefficient in the nth mode and defined by the following:

$$\xi_n = \frac{c_1}{2m\omega_n} = \frac{c_2}{2m{r_g}^2\omega_n} \quad 0 \le \xi_n < 1, \tag{32}$$

here, r_g is the radius of gyration defined by $\sqrt{I_\alpha/m}$; and $F_n(t)$ is calculated as follows:

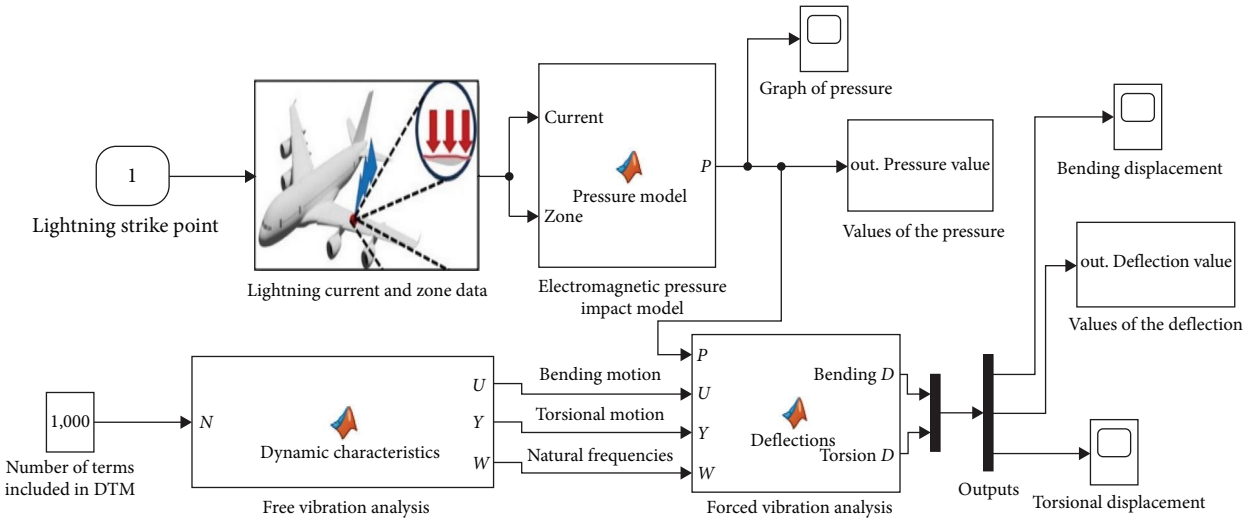

FIGURE 5: MATLAB/Simulink model related with the models established.

$$F_n(t) = \frac{\mu_0}{\mu_n 4\pi^2}\left[\frac{I^{4/3}(t)}{\alpha_0^2\rho_0^{-1/3}t}\int_0^{x_0} U_n(x)dx + I^2(t)\int_{x_0}^{L}\frac{U_n(x)}{(L-x)^2}dx\right], \tag{33}$$

where x_0 is the point where lightning attaches to the aircraft wing exposed to lightning.

By the Duhamel's integral, the solution of Equation (31) is obtained as follows:

$$\begin{aligned} q_n(t) = {} & \exp(-\xi_n\omega_n t)\{A_n\cos(\omega_{nd}t) + B_n\sin(\omega_{nd}t)\} \\ & + \left[\frac{\mu_0}{\mu_n 4\pi^2\omega_{dn}}\int_0^t\left\{\int_0^{x_0-r_c}\frac{U_n(x)}{(x_0-x)^2}dx\right\}\right. \\ & [I_0(\exp(-\alpha_0\tau) - \exp(-\beta_0\tau))]^2 \\ & \exp(-\xi_n\omega_n(t-\tau))\sin(\omega_{nd}(t-\tau))d\tau \\ & + \frac{\mu_0\rho_0^{1/3}}{\mu_n 4\pi^2\alpha_0^2\omega_{dn}}\int_0^t\left\{\int_{x_0-r_c}^{x_0+r_c}U_n(x)dx\right\} \\ & \frac{[I_0(\exp(-\alpha_0\tau) - \exp(-\beta_0\tau))]^{\frac{4}{3}}}{\tau} \\ & \exp(-\xi_n\omega_n(t-\tau))\sin(\omega_{nd}(t-\tau))d\tau \\ & + \frac{\mu_0}{\mu_n 4\pi^2\omega_{dn}}\int_0^t\left\{\int_{x_0+r_c}^{L}\frac{U_n(x)}{(L-x)^2}dx\right\} \\ & [I_0(\exp(-\alpha_0\tau) - \exp(-\beta_0\tau))]^2 \\ & \left.\exp(-\xi_n\omega_n(t-\tau))\sin(\omega_{nd}(t-\tau))d\tau\right], \end{aligned} \tag{34}$$

where A_n and B_n are coefficients related to the initial conditions and ω_{nd} is defined as follows:

$$\omega_{nd} = \omega_n\sqrt{1-\xi_n^2}. \tag{35}$$

Subsequently, substitution of Equation (34) into Equations (28) and (29) gives the general solution for the bending displacement (i.e., bending deflection) and torsional displacement (i.e., torsion deflection) in the aircraft wing with the following forms:

$$u(x,t) = \sum_{n=1}^{N} U_n(x)q_n(t), \tag{36}$$

$$\psi(x,t) = \sum_{n=1}^{N} \Psi_n(x)q_n(t). \tag{37}$$

The MATLAB/Simulink model of the analytical models established is given in Figure 5.

2.3.3. Verification of the Models Established. In the verification of the models established (i.e., the IEPIM and the damage model), the following steps were realized:

(1) The results of the IEPIM were evaluated by using the results of two different experimental studies, borrowed from the open literature, in terms of the relative error.

(2) The results of the damage model were evaluated by using the results of a relevant experimental study, taken from the open literature, in terms of the relative error. In this context, first, the dynamic characteristics of the aircraft wing were obtained in the free vibration analysis. Then, by using the dynamic characteristics, deflections that occurred in the aircraft wing exposed to pressure loading of lightning were obtained in terms of bending deflections and torsion deflections in the forced vibration analysis.

As the material properties of an aircraft wing, the properties of the Goland wing, which were given in Table 5 [55, 56], were considered.

Table 5: Material properties of an aircraft wing.

Material properties of an aircraft wing	
Bending rigidity (EI)	9.75×10^6 Nm^2
Torsional rigidity (GJ)	9.88×10^5 Nm^2
Mass per unit length (m)	35.75 kg/m
Mass moment of inertia per unit length (I_α)	8.65 kg/m
Distance between mass center and shear center (x_α)	0.18 m
Damping coefficient (ξ)	0.01
Length of the wing (L)	6 m

Table 6: Radius of the arc channel at some instants.

Time step (μs)	Lightning current (A)	Length of radius of arc channel of lightning (m)
0	0	0
0.5	50,899	0.00128
1.0	76,968	0.00207
1.5	90,047	0.00268
2.0	96,332	0.00316
2.5	99,066	0.00357
2.6	**99,354**	**0.00365**
3.0	99,948	0.00392

Bold values to highlight the validation by an experimental study that was mentioned in the manuscript.

Table 7: Comparison of the magnitudes of the pressure models for 100 kA lightning current.

	Magnitude of the electromagnetic pressure impact of lightning For 100 kA lightning current						
Time (μs)	IEPIM (Pa)	EMMA [57] (Pa)	Reletive error (%)	SDICOM [57] (Pa)	Reletive error (%)	EPI [11] (Pa)	Relative error (%)
$t = 6$	31.9e + 05	29.6e + 05	7.7	33.1e + 05	3.6	40.1e + 05	20.4
$t = 9$	30.1e + 05	25.1e + 05	19.9	28.1e + 05	7.1	28.1e + 05	7.1
$t = 14$	24.0e + 05	23.7e + 05	1.3	20.5e + 05	17.1	15.2e + 05	57.9
$t = 26$	17.6e + 05	12.4e + 05	41.9	12.0e + 05	46.7	8.3e + 05	112.0

The graphics and results of the models established were realized in the MATLAB/Simulink environment with the codes developed by the user.

3. Results and Discussion

3.1. Verification of the IEPIM. Martins [11] provided an experimental database to understand the direct effects of lightning strikes and validate the lightning arc physical model. The author obtained the value of the electromagnetic pressure impact (EPI) of lightning for 100 kA lightning current by using a current generator. The author showed that for 100 kA lightning current, the radius of the arc channel is about 3.5 mm nearly at $t = 2.6\,\mu$s. About 100 kA lightning current is regarding the component D waveform of lightning as shown in Figure 3. Thus, by using Equation (2), the radius of the arc channel of lightning was found to be reached about 3.6 mm at $t = 2.6\,\mu$s, as shown in Table 6, in the present article. This result proves that the database provided by Martins and the model of the radius of the arc channel of lightning given in Equation (2) are consistent.

In another experimental study, Martins et al. [57] obtained the value of the pressure loading of lightning for different lightning currents by using EMMA and SuperDICOM (SDICOM) lightning high current generators at four instants, $t = 6$, 9, 14, and 26 μs. In this experimental study, the generators were permitted to transmit intense currents by a conduction electrical arc on a test sample connected to a rig made of aluminum plate. The magnitudes of the pressure loading models obtained in the experimental studies and the magnitudes of the IEPIM were evaluated for 100 kA lightning current in Table 7 and for 200 kA lightning current in Table 8, in terms of relative errors at the instants $t = 6$, 9, 14, and 26 μs. As indicated in Tables 7 and 8, it was found that while the results of the IEPIM for 100 kA lightning current are more consistent with the results of certain generators at certain time points, the results of the IEPIM for 200 kA lightning current are more consistent with the results obtained using the generator so-called SDICOM. More precisely, the results of the IEPIM for 100 kA lightning current are closer to the results of SDICOM at $t = 6$ and 9 μs and closer to the results of EMMA at $t = 14$ and 26 μs, as shown in Table 7. On the other hand, the results of the IEPIM for 200 kA lightning current are

Table 8: Comparison of the magnitudes of the pressure models for 200 kA lightning current.

Time (μs)	Magnitude of the electromagnetic pressure impact of lightning For 200 kA lightning current				
	IEPIM (Pa)	EMMA [57] (Pa)	Relative error (%)	SDICOM [57] (Pa)	Relative error (%)
$t=6$	37.6e+05	36.3e+05	3.6	40.7e+05	7.6
$t=9$	36.5e+05	32.4e+05	12.7	36.3e+05	0.6
$t=14$	32.8e+05	27.3e+05	20.1	30.2e+05	8.6
$t=26$	21.9e+05	20.9e+05	4.8	22.1e+05	0.9

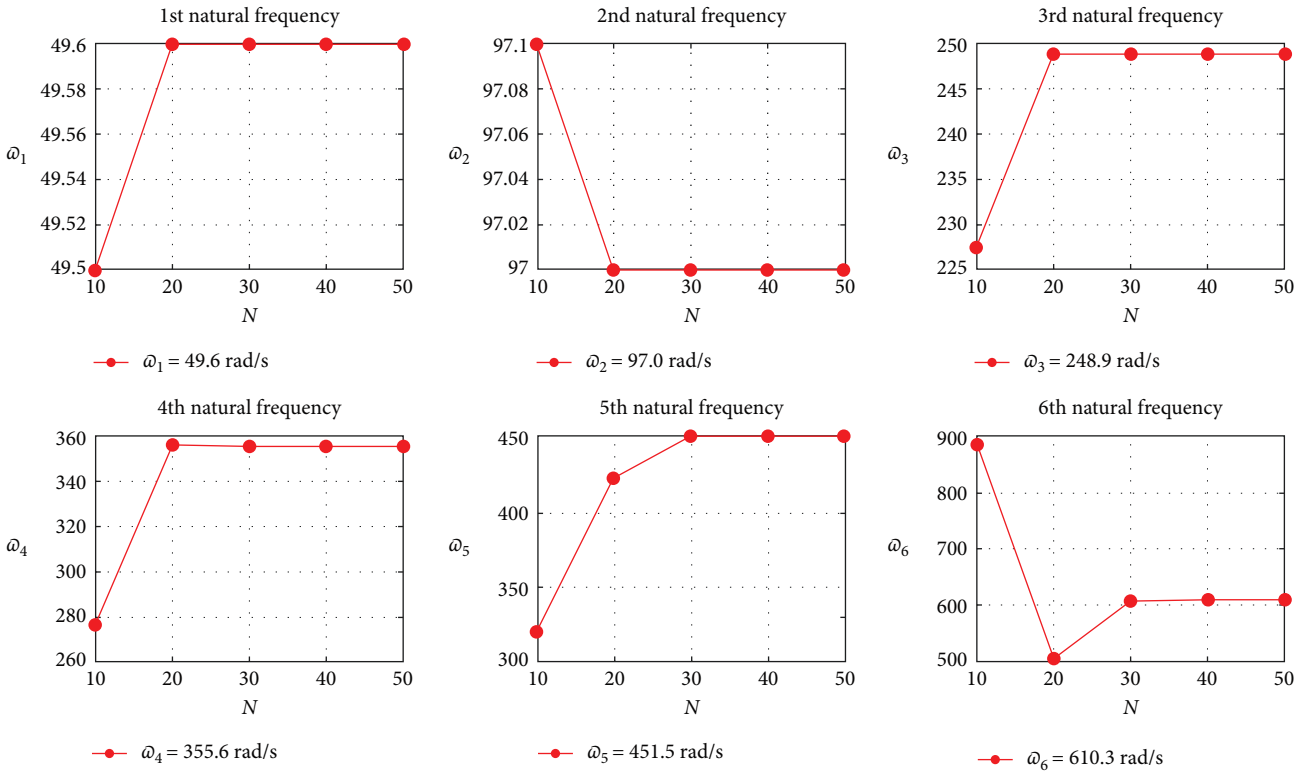

Figure 6: Convergence of the first six vibration frequencies of the aircraft wing with respect to N (N: number of terms included in DTM).

closer to the result of EMMA at $t=6$ μs and closer to the results of SDICOM at $t=9$, 14, and 26 μs, as shown in Table 8. Here, it can be noticed that the results of the IEPIM are quite consistent with the results of two experimental studies up to the first 26 μs for 100 kA lightning current. At the 26th microsecond, the amount of the relative error was found to be relatively higher. Since 100 kA lightning current is associated with a short-duration component D waveform with a rise time of up to 25 μs [10], the relative error at $t=26$ μs for 100 kA lightning current can be neglected. This proves that the component D waveform is valid before 26 μs. In contrast, it is seen that the results of the IEPIM are quite consistent with the results of the experimental study for 200 kA lightning current because 200 kA lightning current is associated with component A waveform, as shown in Figure 2, with a rise time of less than 50 μs [10].

3.2. Verification of the Damage Model

3.2.1. Results of the Free Vibration Analysis. In the free vibration analysis, first, the convergence of the vibration frequencies of the aircraft wing was determined, as shown in Figure 6. In Figure 6, it can be seen that only the first thirty terms of DTM are required to get the first six convergent vibration frequencies. Subsequently, the vibration frequencies obtained were compared with the vibration frequencies found in [55] in terms of relative error ε. It was found that the results of DTM were found to converge to the results of the vibration frequencies found in [55] with almost zero relative error, as given in Table 9.

Then, by using the vibration frequencies, the vibration mode shapes of the aircraft wing were obtained, as depicted

Table 9: The first six vibration frequencies of the aircraft wing.

	Vibration freq. (rad/s) (ω_n)	ω_{Ref} [55]	ω_{DTM} ($N = 30$)	ε (%)
Goland wing	ω_1	49.6	49.6	0.00
	ω_2	97.0	97.0	0.00
	ω_3	248.9	248.9	0.00
	ω_4	355.6	355.6	0.00
	ω_5	451.5	451.5	0.00
	ω_6	610.1	610.3	0.03

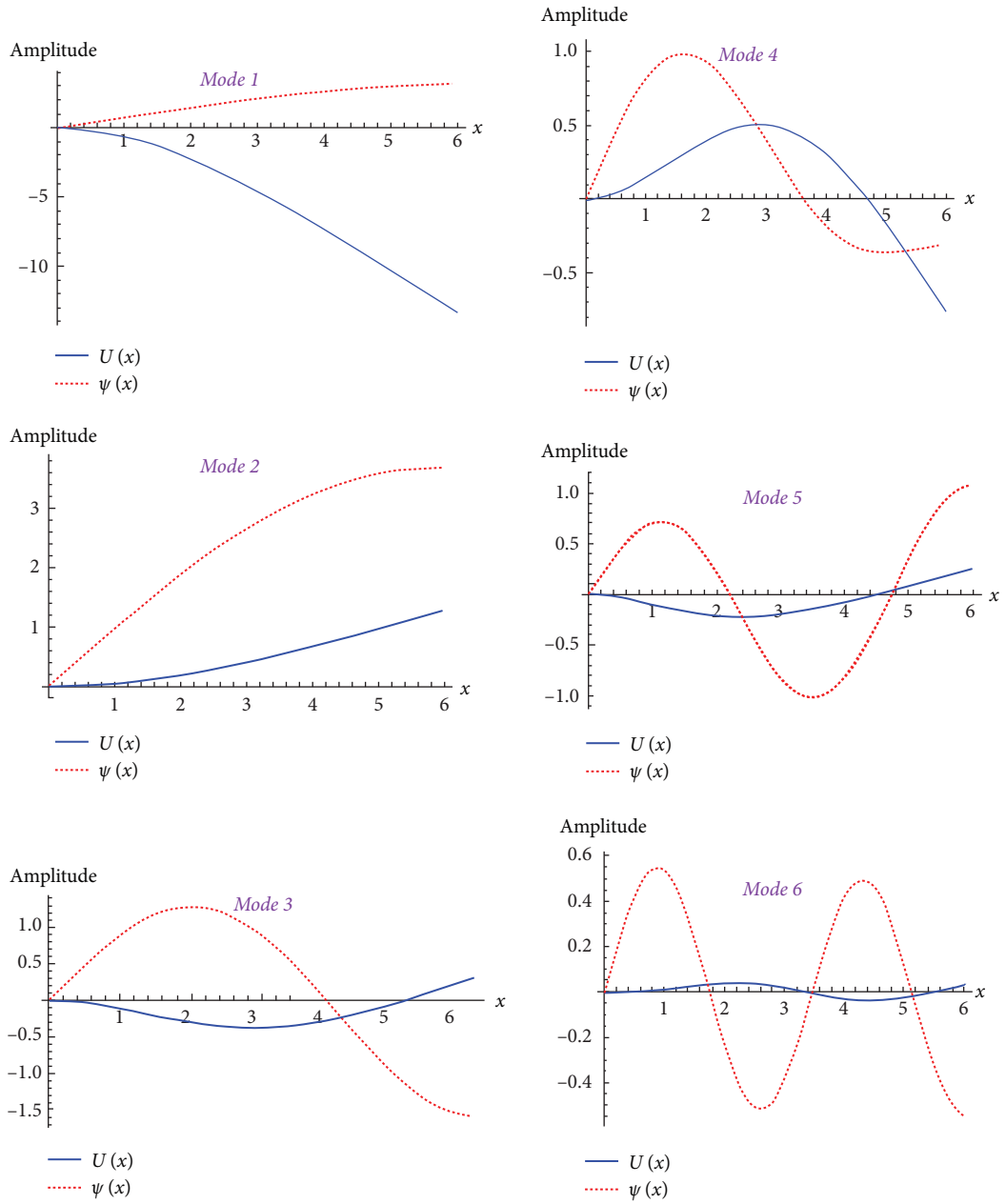

Figure 7: The first six vibration mode shapes of the aircraft wing.

Table 10: Amount of bending deflection in an aircraft wing at different locations (x_0) with respect to damping coefficient (ξ).

Bending deflections at lightning strike point in Zone 2A (mm) (ξ vs x_0)			
Zone 2A (ξ/x_0)	Wing root ($x_0 = 0.5$ m)	Mid-wing ($x_0 = 3.0$ m)	Wing tip ($x_0 = 4.5$ m)
$\xi = 0$	0.2118	3.1086	9.5246
$\xi = 0.0050$	0.2114	3.1050	9.5140
$\xi = 0.01$	0.2110	3.1016	9.5038
$\xi = 0.0150$	0.2106	3.0982	9.4932
$\xi = 0.02$	0.2103	3.0950	5.4840

Table 11: Amount of torsion deflection in an aircraft wing at different locations (x_0) with respect to damping coefficient (ξ).

Torsion deflections at lightning strike point in Zone 2A (mm) (ξ vs x_0)			
Zone 2A (ξ/x_0)	Wing root ($x_0 = 0.5$ m)	Mid-wing ($x_0 = 3.0$ m)	Wing tip ($x_0 = 4.5$ m)
$\xi = 0$	0.8884	1.9895	2.3523
$\xi = 0.0050$	0.8875	1.9883	2.3497
$\xi = 0.01$	0.8866	1.9871	2.3471
$\xi = 0.0150$	0.8858	1.9859	2.3445
$\xi = 0.02$	0.8849	1.9848	2.3422

in Figure 7. Compared with the vibration mode shapes obtained in [55], a good agreement was found between the present article and the reference.

3.2.2. Results of the Forced Vibration Analysis. Martins, in the experimental study [11], found that when the pressure impact of lightning, including 100 kA lightning current, was applied to the center of a pure aluminum panel, the maximal amplitude of the deflection in the lateral direction was found about 3.1 mm approximately at $t = 1$ ms, which is larger than the duration of mechanical action. Then, the author explained that the deflection at the center of the panel continues to increase without arc. This suggests that deflection at the center of the panel arises after the mechanical action time. In the present article, the center of the aircraft wing is the mid-wing ($x_0 = 3$ m), which is in Zone 2A associated with approximately 100 kA lightning current, as shown in Figure 2 and Table 4. In the defection model, when the impact point for 100 kA lightning current was taken as $x_0 = 3$ m (i.e., the mid-wing) from the leading edge, the bending deflection was found about 3.1 mm at $t = 20\ \mu$s depending on the value of the damping coefficient, as shown in Table 10. This proves that the result of the damage model for the mid-wing is consistent with the result of the experimental study provided by Martins. Furthermore, when the impact point for 100 kA lightning current was also taken as $x_0 = 0.5$ (wing-root) and $x_0 = 4.5$ (wing tip), that are in Zone 2A, the deflections occurred in these regions were about 0.2 and 9.5 mm at $t = 20\ \mu$s, respectively, as shown in Table 10. This indicates that when the impact point approaches to the wing tip, the deflection occurred in the wing increases; on the other hand, when the impact point approaches to the wing root, the deflection occurred in the wing decreases. In addition, in Table 10, it was seen that when the lightning strike point (x_0) is fixed, and the damping coefficient (ξ) is increased in the range of $[0, 2\xi]$, the amount of deflection decreases as the amount of damping coefficient increases.

Regarding the torsion deflections in the aircraft wing, Table 11 shows that the torsion deflection for 100 kA lightning current is about 0.8 mm in the wing root, is about 1.9 mm in the mid-wing and is about 2.3 mm in the wing tip at $t = 20\ \mu$s. Furthermore, as in Table 10, when the impact point moves to the wing tip, the deflection arisen in the wing increases; by contrast, when the impact point moves to the wing root, the deflection arisen in the wing decreases. In addition, when the damping coefficient is increased in the interval $[0, 2\xi]$, the amount of deflection in the wing decreases. Considered Tables 10 and 11, it can be concluded that when lightning, including 100 kA current, hits to the wing root of an aircraft, the pressure impact of the lightning causes more torsion deflection than bending deflection at the wing root; conversely, when lightning with a current of 100 kA hits to the mid-wing or wing tip of an aircraft, the pressure impact of the lightning causes more bending deflection than torsion deflection at the mid-wing or wing tip.

The deflected shapes of the aircraft wing in the form of bending displacement (bending deflection) and torsional displacement (torsion deflection) were given for the wing root, mid-wing, and wing tip, respectively, in Figure 8. As shown in Figure 8(b), the deflected shape of the wing exposed to a lightning strike at the mid-wing is in the form of a damped sine wave, as in the experimental study [11].

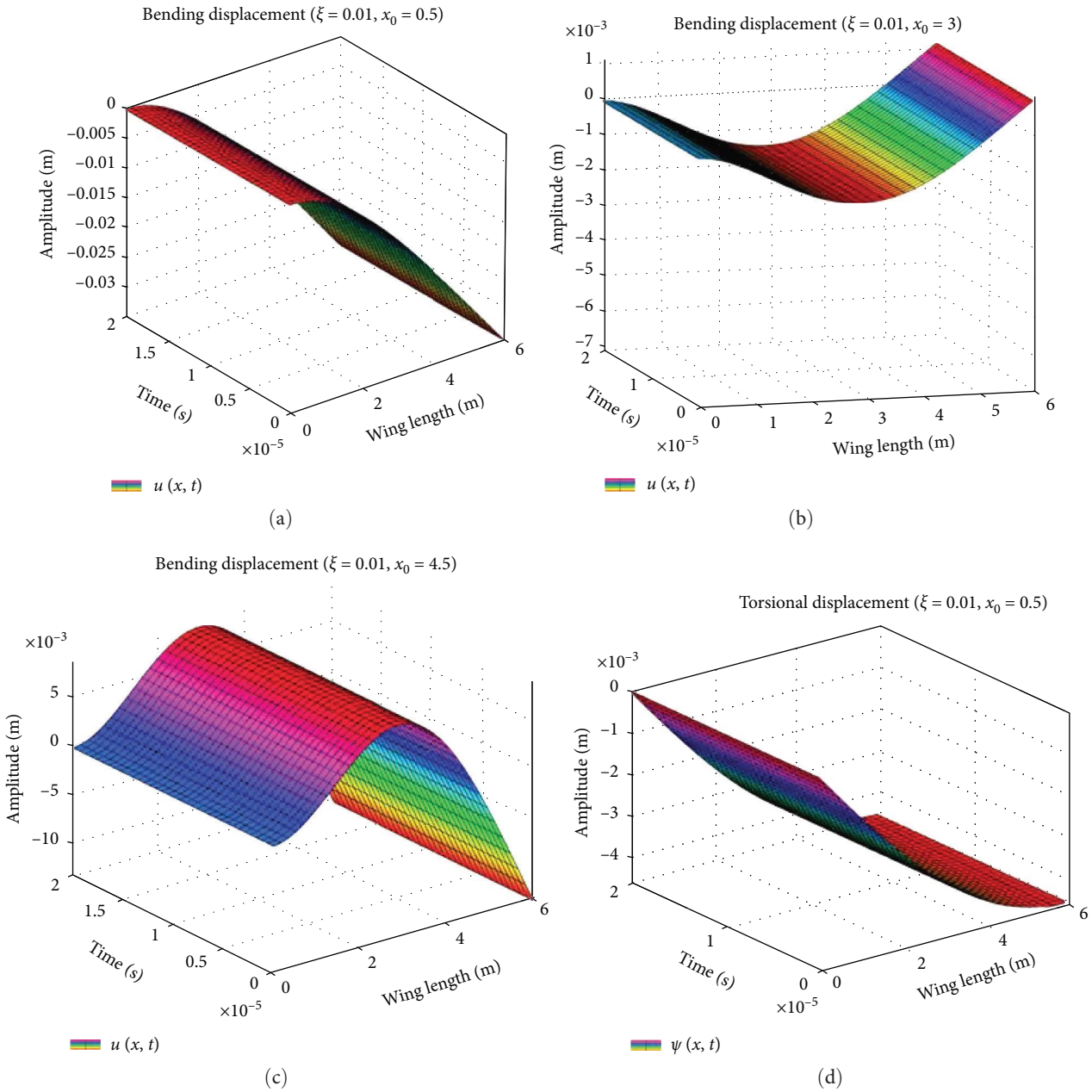

Figure 8: Continued.

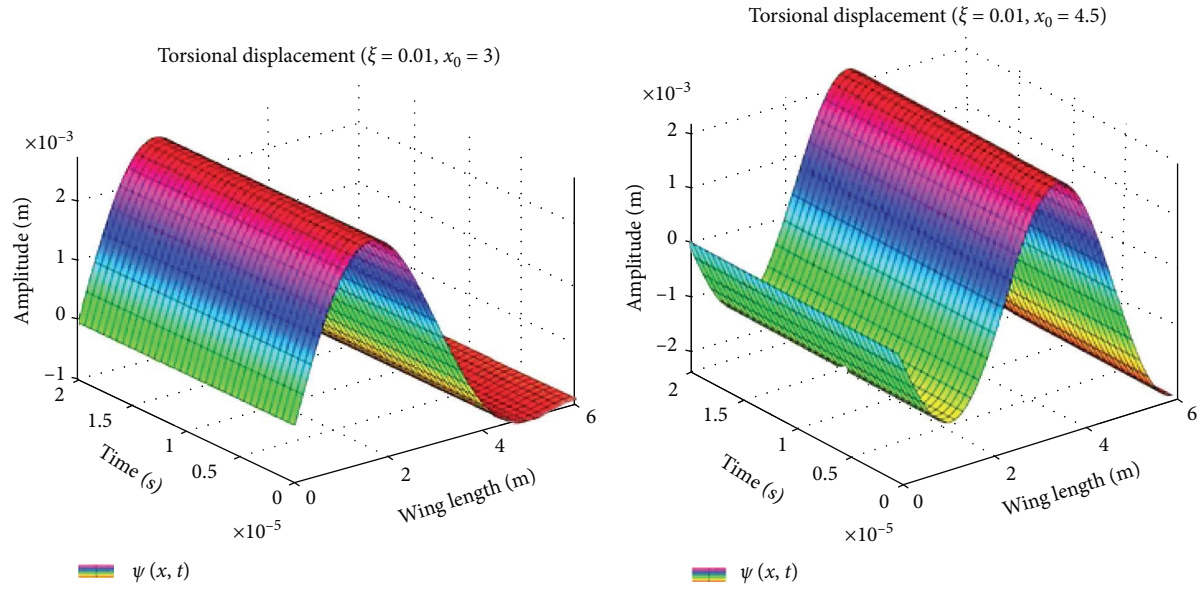

FIGURE 8: (a–f) The deflected shapes of the aircraft wing when lightning hits to the wing root (at $x_0 = 0.5$), mid-wing (at $x_0 = 3$), and wing tip (at $x_0 = 4.5$).

4. Conclusion

Damages induced by lightning strikes in aircraft structural materials with high thermal and electrical conductivity are mostly caused by the electromagnetic pressure loading of lightning, which is the lateral pressure effect of lightning. In the present article, the lightning-induced damage behavior of an aircraft structural material is investigated analytically. For this purpose, two analytical-based models were developed: an IEPIM and a damage model. To validate the models established, the results of the models were compared with the results of relevant experimental studies from the open literature.

The findings of the present article concluded that:

(1) The results of the lightning pressure model proposed (i.e., IEPIM) are quite consistent with the results of two experimental studies for 100 kA lightning current and 200 kA lightning current.

(2) Although lightning hits to regions with the same characteristics on an aircraft wing in terms of the lightning strike zone, the amount of deflection caused by the pressure impact of lightning on the wing increases as the impact point approaches the wing tip and decreases as it approaches the wing root.

(3) When the lightning strike point (x_0) is fixed, and the damping coefficient (ξ) is increased in the range of $[0, 2\xi]$, the amount of deflection decreases as the amount of damping coefficient increases.

(4) When lightning including 100 kA current hits to the wing root of an aircraft, the pressure impact of the lightning causes more torsion deflection than bending deflection at the wing root; in contrast, when lightning including 100 kA current hits to the mid-wing or wing tip of an aircraft, the pressure impact of the lightning causes more bending deflection than torsion deflection at the mid-wing or wing tip.

Based on the results obtained in this article, it was found that the theoretical results of the article are in good agreement with the results of the experimental studies in the literature. However, considering today's laboratory conditions and the current state of advanced computer simulations, it is recommended that the models established in the present article be retested before implementation.

Data Availability

The data obtained as the findings of this study were described in the current study at the scale deemed appropriate by the authors of the study.

Conflicts of Interest

The authors declare that they have no known competing financial interests or personal relationships that could have appeared to influence the work reported in this paper.

References

[1] J. Plumer and J. Robb, "The direct effects of lightning on aircraft," *IEEE Transactions on Electromagnetic Compatibility*, vol. EMC-24, no. 2, pp. 158–172, 1982.

[2] C. Guerra-Garcia, N. C. Nguyen, J. Peraire, and M. Martinez-Sanchez, "Charge control strategy for aircraft-triggered lightning strike risk reduction," *AIAA Journal*, vol. 56, no. 5, pp. 1988–2002, 2018.

[3] E. Brian-Curran, R. L. Holle, and R. E. López, "Lightning casualties and damages in the United States from 1959 to 1994," *Journal of Cimate*, vol. 13, pp. 3448–3464, 2000.

[4] Y. He, X. Yue, S. Lindbergh, J. Gao, C. Graves, and J. Rakas, "Dissecting lightning strike hazard impact patterns to National Airspace System facilities in the contiguous United States," *Computers, Environment and Urban Systems*, vol. 91, Article ID 101735, 2022.

[5] P. Feraboli and H. Kawakami, "Damage of carbon/epoxy composite plates subjected to mechanical impact and simulated lightning," *Journal of Aircraft*, vol. 47, no. 3, pp. 999–1012, 2010.

[6] C. Karch, F. Heidler, and C. Paul, "Protection of aircraft radomes against direct lightning strikes—an overview," *Atmosphere*, vol. 12, no. 9, Article ID 1141, 2021.

[7] A. Temnikov, L. Chernensky, O. Belova et al., "Influence of kind of lightning stripe models on spectral characteristics of discharge phenomena inside aircraft nose radome model," *Journal of Electrostatics*, vol. 115, Article ID 103661, 2022.

[8] J. Langot, E. Gourcerol, A. Serbescu et al., "Performance of painted and non-painted non-woven nickel-coated carbon fibers for lightning strike protection of composite aircraft," *Composites Part A: Applied Science and Manufacturing*, vol. 175, Article ID 107772, 2023.

[9] L. Gebrehiwet, E. Abeselom, E. Abate, Y. Negussie, and T. Teklehaymanot, "Application of composite materials in aerospace & automotive industry: review," *International Journal of Advances in Engineering and Management (IJAEM)*, vol. 5, Article ID 697, 2023.

[10] H. Kawakami, *Lightning strike induced damage mechanisms of carbon fiber composites*, University of Washington, 2011.

[11] R. S. Martins, *Experimental and theoretical studies of lightning arcs and their interaction with aeronautical materials*, https://hal.science/tel-01434026, Universite Paris-Saclay, 2016.

[12] C. Karch, A. Arteiro, and P. P. Camanho, "Modelling mechanical lightning loads in carbon fibre-reinforced polymers," *International Journal of Solids and Structures*, vol. 162, pp. 217–243, 2019.

[13] R. Muñoz, S. Delgado, C. González, B. López-Romano, D.-Y. Wang, and J. Llorca, "Modeling lightning impact thermo-mechanical damage on composite materials," *Applied Composite Materials*, vol. 21, no. 1, pp. 149–164, 2014.

[14] J. Lee, T. E. Lacy Jr., and C. U. Pittman Jr, "Coupled thermal electrical and mechanical lightning damage predictions to carbon/epoxy composites during arc channel shape expansion," *Composite Structures*, vol. 255, pp. 2–19, 2021.

[15] L. Chemartin, P. Lalande, B. Peyrou et al., "Direct effects of lightning on aircraft structure: analysis of the thermal, electrical and mechanical constraints," *Aerospace Lab*, vol. 5, pp. 1–15, 2012.

[16] J. Y. Lee and G. J. Collins, "Risk analysis of lightning effects in aircarft systems," in *2017 IEEE Aerospace Conference*, pp. 1–9, IEEE, Big Sky, MT, USA, 2017.

[17] L. Meirovitch and I. Tuzcu, *Integrated Approach to the Dynamics and Control of Maneuvering Flexible Aircraft*, NASA, 2003.

[18] A. Alsahlani, T. Rahulan, and N. Abdulhassan, "Composite structural analysis of a high altitude, solar powered unmanned aerial vehicle," *International Journal of Mechanical Engineering and Robotics Research*, vol. 6, no. 1, pp. 71–76, 2017.

[19] F. Wang, X. Ma, Z. Wei, Y. Wu, and C. Huang, "Lightning damage of composite material driven by multi-physics coupling," *Composites Science and Technology*, vol. 233, Article ID 109886, 2023.

[20] M. Damghani, J. Saddler, E. Sammon, G. A. Atkinson, J. Matthews, and A. Murphy, "An experimental investigation of the impact response and post-impact shear buckling behaviour of hybrid composite laminates," *Composite Structures*, vol. 305, Article ID 116506, 2023.

[21] D. Boushab, P. Gharghabi, J. Lee et al., "Lightning arc channel effects on surface damage development on a PRSEUS composite panel: an experimental study," *Composites Part B: Engineering*, vol. 224, Article ID 109217, 2021.

[22] J. M. Guerrero, A. Sasikumar, J. Llobet, and J. Costa, "Experimental and virtual testing of a composite-aluminium aircraft wingbox under thermal loading," *Aerospace Science and Technology*, vol. 138, Article ID 108329, 2023.

[23] J. Lee, T. E. Lacy Jr., C. U. Pittman Jr., and J. N. Reddy, "Numerical estimations of lightning-induced mechanical damage in carbon/epoxy composites using shock wave overpressure and equivalent air blast overpressure," *Composite Structures*, vol. 224, Article ID 111039, 2019.

[24] P. Foster, G. Abdelal, and A. Murphy, "Quantifying the influence of lightning strike pressure loading on composite specimen damage," *Applied Composite Materials*, vol. 26, no. 1, pp. 115–137, 2019.

[25] A. Bigand, C. Espinosa, and J. M. Bauchire, "Equivalent mechanical load model methodology to simulate lightning strike impact on protected and painted composite structure," *Composite Structures*, vol. 280, Article ID 114886, 2022.

[26] Y.-F. Qian, Z.-F. Ye, and H.-B. Zhang, "Impact of modeling simplifications on lightning strike simulation for aeroengine," *Mathematical Problems in Engineering*, vol. 2019, Article ID 5176560, 11 pages, 2019.

[27] F. Lago, "Lightning in aeronautics," *Journal of Physics: Conference Series*, vol. 550, Article ID 012001, 2014.

[28] A. Larsson, "The interaction between a lightning flash and an aircraft in flight," *Comptes Rendus Physique*, vol. 3, no. 10, pp. 1423–1444, 2002.

[29] A. Soysal, İ. Özkol, and E. Uzal, "Investigation of the behavior of an aircraft wing exposed to lightning strike with an analytical-based model," in *2023 10th International Conference on Recent Advances in Air and Space Technologies (RAST)*, pp. 1–15, IEEE, Istanbul, Turkiye, 2023.

[30] G. Sweers, B. Bruce, and G. John, "Lightning strikes: protection, inspection, and repair," *Aero Magazine*, vol. 4, pp. 19–28, 2012.

[31] M. Gagné and D. Therriault, "Lightning strike protection of composites," *Progress in Aerospace Sciences*, vol. 64, pp. 1–16, 2014.

[32] Y. Wang and O. I. Zhupanska, "Lightning strike thermal damage model for glass fiber reinforced polymer matrix composites and its application to wind turbine blades," *Composite Structures*, vol. 132, pp. 1182–1191, 2015.

[33] A. C. Garolera, *Lightning Protection of Flap System for Wind Turbine Blades*, DTU Elektro, 2014.

[34] C. E. Rash, "When lightning strikes," *AeroSafety World*, vol. 5, pp. 18–23, 2010.

[35] U. Sonnadara, V. Kathriarachchi, V. Cooray, R. Montano, and T. Götschl, "Performance of lightning locating systems in extracting lightning flash characteristics," *Journal of Atmospheric and Solar-Terrestrial Physics*, vol. 112, pp. 31–37, 2014.

[36] A. A. Baker, "Repair of cracked or defective metallic aircraft components with advanced fibre composites—an overview of Australian work," *Composite Structures*, vol. 2, no. 2, pp. 153–181, 1984.

[37] D. Mitchard, N. S. Jamoshid, C. Stone, and A. Haddad, "Experimental and theoretical evaluation of aluminium

deflection due to lightning strikes," in *2016 33rd International Conference on Lightning Protection (ICLP)*, pp. 1–6, IEEE, Estoril, Portugal, September 2016.

[38] W. Radasky and E. Savage, "Intentional Electromagnetic Interference (IEMI) and its impact on the U.S. Power Grid," *Metatech*, vol. 1, pp. 1–3, 2010.

[39] F. Treyssède, "Vibration analysis of horizontal self-weighted beams and cables with bending stiffness subjected to thermal loads," *Journal of Sound and Vibration*, vol. 329, no. 9, pp. 1536–1552, 2010.

[40] G. Liu, D. Guo, Z. Lin et al., "Exceeding 50% injected lightning energy not sourced: during the analysis of an OGW rupture accident caused by multiple lightning strikes," *Engineering Failure Analysis*, vol. 143, Article ID 106779, 2023.

[41] D. Guo, G. Liu, H. Chen, P. Wang, and X. Lin, "Influence of structural characteristics for overhead ground wire on arc root under lightning strike," *Electrical Engineering*, vol. 105, no. 5, pp. 3283–3292, 2023.

[42] G. Liu, X. Peng, M. Zhong et al., "A case study of ruptures in overhead ground wire under a large lightning over 400 kA," *Engineering Failure Analysis*, vol. 104, pp. 1211–1233, 2019.

[43] C. E. S. Cesnik and E. Brown, "Active warping control of a joined- wing airplane configuration," in *44th AIAA/ASME/ASCE/AHS/ASC Structures, Structural Dynamics, and Materials Conference*, pp. 1–15, AIAA, Norfolk, Virginia, 2003.

[44] M. J. Patil and D. H. Hodges, "On the importance of aerodynamic and structural geometrical nonlinearities in aeroelastic behavior of high-aspect-ratio wings," *Journal of Fluids and Structures*, vol. 19, no. 7, pp. 905–915, 2004.

[45] J. R. Dwyer and M. A. Uman, "The physics of lightning," *Physics Reports*, vol. 534, no. 4, pp. 147–241, 2014.

[46] L. Chemartin, P. Lalande, E. Montreuil, C. Delalondre, B. G. Chéron, and F. Lago, "Three dimensional simulation of a DC free burning arc. Application to lightning physics," *Atmospheric Research*, vol. 91, no. 2–4, pp. 371–380, 2009.

[47] D. A. Xu, M. N. Shneider, D. A. Lacoste, and C. O. Laux, "Thermal and hydrodynamic effects of nanosecond discharges in atmospheric pressure air," *Journal of Physics D: Applied Physics*, vol. 47, no. 23, Article ID 235202, 2014.

[48] K. Fu and L. Ye, "Modelling of lightning-induced dynamic response and mechanical damage in CFRP composite laminates with protection," *Composite Structures*, vol. 218, pp. 162–173, 2019.

[49] L. Zhang, J. Mu, H. Ma, G. Dai, and S. Tong, "Research on fault-tolerant control of combined airframe damage of electric aircraft," *Aerospace*, vol. 10, no. 7, Article ID 611, 2023.

[50] V. Kumar, T. Yokozeki, C. Karch et al., "Factors affecting direct lightning strike damage to fiber reinforced composites: a review," *Composites Part B: Engineering*, vol. 183, Article ID 107688, 2020.

[51] J. K. Zhou, *Differential Transformation and Its Applications for Electrical Circuits*, Huazhong University Press, Wuhan, 1986.

[52] A. Soysal, İ. Özkol, and E. Uzal, "Flexural–torsional-coupled vibration analysis of Euler–Bernoulli beam by using the differential transform method," *Academic Perspective Procedia*, vol. 5, no. 3, pp. 26–33, 2022.

[53] S. H. R. Eslimy-Isfahany and J. R. Banerjee, "Dynamic response of an axially loaded bending–torsion coupled beam," *Journal of Aircraft*, vol. 33, no. 3, pp. 601–607, 1996.

[54] S. H. R. Eslimy-Isfahany, J. R. Banerjee, and A. J. Sobey, "Response of a bending–torsion coupled beam to deterministic and random loads," *Journal of Sound and Vibration*, vol. 195, no. 2, pp. 267–283, 1996.

[55] S. H. R. Eslimy-Isfahany and J. R. Banerjee, "Use of generalized mass in the interpretation of dynamic response of bending–torsion coupled beams," *Journal of Sound and Vibration*, vol. 238, no. 2, pp. 295–308, 2000.

[56] R. S. Martins, C. Zaepffel, L. Chemartin, P. Lalande, and F. Lago, "Characterization of high-current pulsed arcs ranging from 100–250 kA peak," *Journal of Physics D: Applied Physics*, vol. 52, no. 18, Article ID 185203, 2019.

[57] H. Kawakami and P. Feraboli, "Lightning strike damage resistance and tolerance of scarf-repaired mesh-protected carbon fiber composites," *Composites Part A: Applied Science and Manufacturing*, vol. 42, no. 9, pp. 1247–1262, 2011.